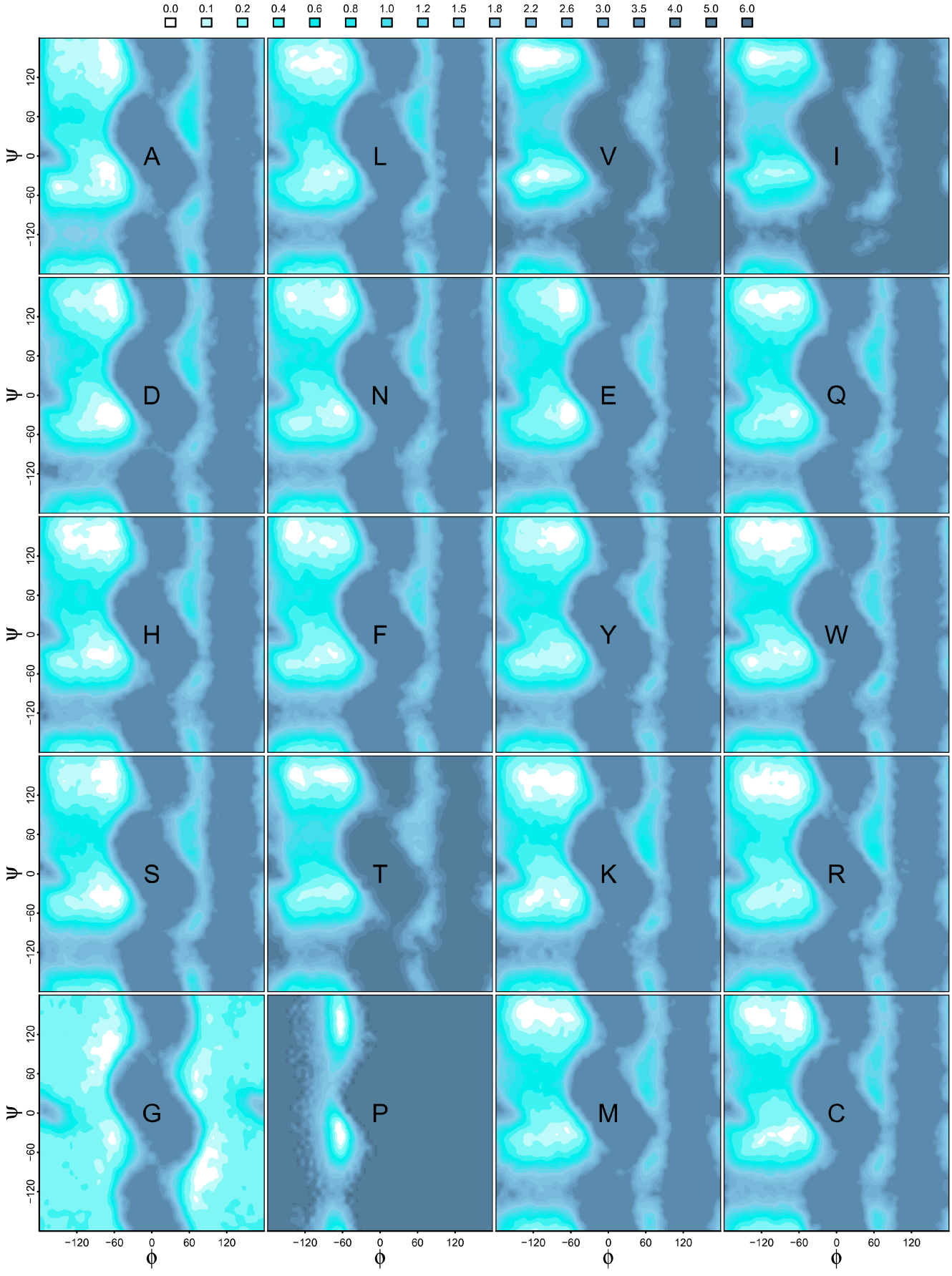
0.0 0.1 0.2 0.4 0.6 0.8 1.0 1.2 1.5 1.8 2.2 2.6 3.0 3.5 4.0 5.0 6.0
A
L
V
I
D
N
E
Q
H
F
Y
W
S
T
K
R
G
P
M
C
ψ
ϕ
120
60
0
−60
−120

FIGURE S1: Statistical potential used during sampling. For the various amino acids indicated by their one letter code, we show the effective potential in use during the simulation as two-dimensional color maps. The plots are created at finer resolution (1°) compared to the tabulated values they are constructed from (resolution of 6°). This means that they do reflect the interpolation protocol in use, which in general employed fourth-order B-splines rather than an exact, interpolating spline to achieve a smoother surface (except for proline). Note that the low likelihood regions are flattened to prevent the introduction of uncrossable barriers at the backbone level. For the sterically feasible envelope for negative ϕ-values, the potentials are all rather featureless. The color legend given on top applies to all panels. It has units of kcal/mol and lists for each color level its boundary toward lower energies.

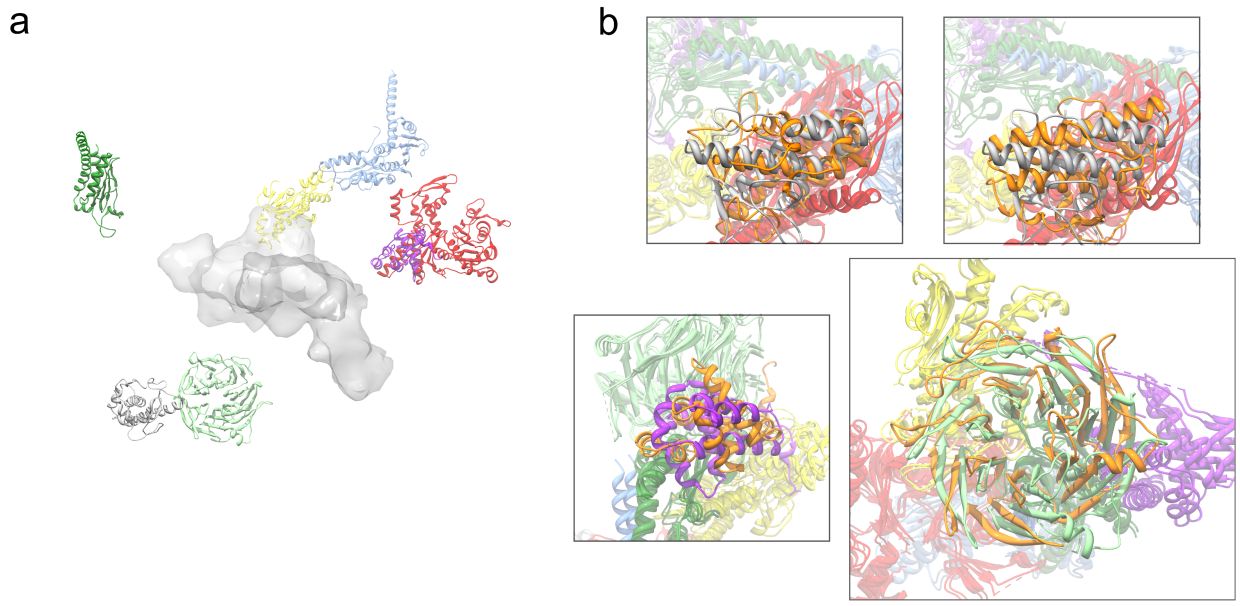

FIGURE S2: Auxiliary data for the Arp2/3 system (Nolen et al., 2004). **a**. A single random starting structure for an individual replica in one of the replica exchange simulations. Note that all starting structures for all replicas and all runs are different. The color code is the same as in Fig. 1, and the input density is shown for reference. **b**. Visualization of 4 non-native centroid snapshots of clusters for the Arp2/3 sampling at the lowest input resolution ($A_g = 17$, clusters at least 1% in size). Each panel highlights only the relevant portion of the assembly, and arrangement is by decreasing cluster size from top-left to right-bottom. The incorrect conformation of the chain in question is highlighted in orange. All cases involve rotation of a domain in place, and it is expected that these errors occur at low resolution and predominantly for roughly spherical chains. Images were generated with UCSF Chimera (Pettersen et al., 2004).

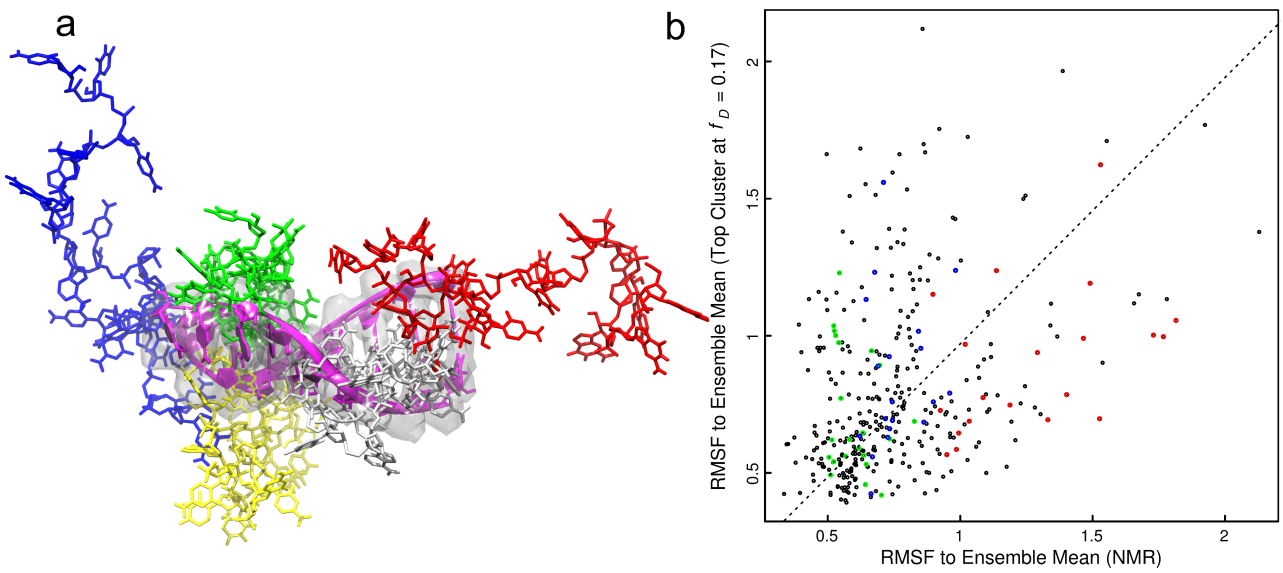

FIGURE S3: Auxiliary data for the RNA stem-loop (Chang and Nikonowicz, 2012). **a**. Five different starting structures (blue, yellow, gray, red, and green) used for individual replicas in the simulations are shown. Since these structures are randomly generated at the dihedral angle level, they have no relationship whatsoever with either the density (transparent envelope) or the NMR ensemble (first model shown in magenta). The image was generated with UCSF Chimera. **b**. For the high resolution run ($A_g = 2$) and highest restraint strength ($f_D = 0.17$), the largest and native-like cluster encompasses 17933/29600 snapshots. It was considered as an ensemble and root-mean square fluctuation (RMSF) values were computed for all heavy atoms with respect to the mean. The same was done for the 8 structures in the NMR ensemble. The resultant values were plotted against each other in units of Å. Colors highlight 3 specific residues, *viz*., A4 (green), C9 (red), and C17 (blue). The color annotation reveals that the relationship between the data sets is weak, *i.e*., residues that are qualitatively different by NMR assessment populate RMSF values for the simulated ensemble, which are only marginally different. Nevertheless, reasonable agreement is found for the overall range of values and their distribution. The dashed line is a linear fit constrained to pass through the origin (slope is 0.97).

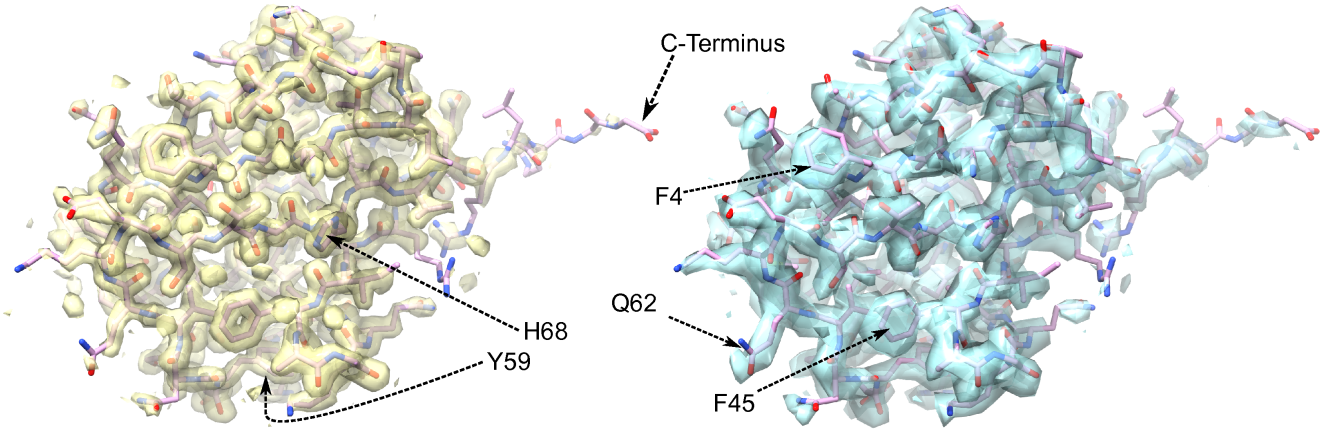

FIGURE S4: Comparison of original and processed input densities. The original input density (clipped to reveal the central ubiquitin molecule of the unit cell) is shown on the left as an encapsulating surface with numerical value 0.621 (Vijay-Kumar et al., 1987). Using an identical viewpoint and magnification, the interpreted input density is shown on the right. For $\omega_I = -0.20$ and $\rho_{sol} = 1.01\ \mathrm{g\,cm^{-3}}$, the surface shown corresponds to a physical density level of approximately $1.8\ \mathrm{g\,cm^{-3}}$. The view is from the β-sheet side of ubiquitin, and several, predominantly aromatic side chains are highlighted (using one-letter code). Aside from the obvious change in resolution, skew can be introduced by the binning filter (*e.g.*, seen for F4). It is also apparent that conformational averaging even with small amplitude will lead to reductions in apparent density, and this is visible for the C-terminus and many surface-exposed side chains. Images were generated with UCSF Chimera using its volume viewer.

SUPPLEMENTAL EXPERIMENTAL PROCEDURES

PROCESSING OF INPUT DENSITY (related to Experimental Procedures and Results – Restraining Molecular Simulations to a Target Mass Density – *Processing of Experimental Input Densities*)

As outlined in the main text, we cannot and do not want to make overly specific assumptions about the relationship of input data and the physical matter they are assumed to be generated by. This leaves a standard linear approach as the simplest model. Rather than minimizing model-based deviations or using correlation coefficients directly, our linear transform is meant to generate an interpreted density map that is physically reasonable. To do this, we enforce that the background level in the interpreted map coincides with the user-selected value for the (positive) physical background density, ρ_{sol}, that is also used in eq. 2 in the main text. The values differing from the background signal are then scaled in parameter-dependent fashion.

In agreement with standard procedures found in the literature, we need to find or define the signal level corresponding to background in the input density, and we term this quantity ω_{bg}. The value for ω_{bg} can either be set manually, or it can be obtained from a histogram of the individual values of ω for all lattice cells. In the latter case, the position of the highest peak is typically associated with ω_{bg}. The key parameter is a threshold level for the input density, ω_t, which is meant to distinguish signals associated with the molecule(s) of interest from background. We use it to evaluate two sums:

$$\begin{aligned} V_M &= \sum_i \sum_j \sum_k \mathrm{H}(\omega_{ijk} - \omega_t)\, V_{ijk} \\ E_M &= \sum_i \sum_j \sum_k \mathrm{H}(\omega_{ijk} - \omega_t)\left[\omega_{ijk} - \omega_{bg}\right] V_{ijk} \end{aligned} \qquad \text{(S1)}$$

Here, H(x) denotes the Heaviside step function, and quantities V_M and E_M correspond to the total volume and integrated excess signal of the solute matter, respectively. The threshold parameter effectively defines the scaling component of the linear transform. It does not, however, imply that any signal in the input density below this value is later discarded or disregarded otherwise. This is

important because the contrast levels in the input density may be heterogeneous, and discarding signals upfront could lead to loss of important information. The integrated quantities are used in conjunction with the assumed total mass of the solute matter, M_M, as follows:

$$c_2 = \frac{M_M - \rho_{sol} V_M}{E_M} \tag{S2}$$

Eq. S2 essentially compares a predicted excess signal with the actual excess integral to determine the scaling factor used in the final result for the interpreted density:

$$\Xi_{ijk} = \rho_{sol} + c_2 \left(\omega_{ijk} - \omega_{bg} \right) \tag{S3}$$

The critical parameter, ω_t, must be chosen such that $\rho_M = M_M / V_M$ is larger than the physical background density. This poses a fairly delicate constraint on ω_t that can already be helpful in interpreting an input map. It also alludes to the fact that the identity of the solute matter generating the signal must be known with some amount of precision. In general, this is not a trivial issue due to the complications incurred by data averaging in conjunction with sample heterogeneities as discussed in the main text.

SAMPLING METHODOLOGY (related to Experimental Procedures and Results – Sampling Methodology)

Hybrid Sampling Protocol

In this study, we use a hybrid Monte Carlo (MC) and mixed rigid-body / internal coordinate space dynamics (IMD) sampling protocol, in which short runs of dynamics are interspersed with MC segments (Vitalis and Pappu, 2009). The motivation for this lies in the fact that the density restraint potential (eq. 4 in the main text) can create a very detailed and rugged energy surface requiring high levels of correlation for structural relaxation while also being prone to conformational trapping. The former is supposed to be provided by the force-based portion of the sampling engine, while the latter is hopefully addressed by conformational jumps made possible by MC moves. Below, we will first discuss caveats before describing the implementation and finishing up by providing some statistics for

assessment.

As for caveats, a trajectory resulting from a hybrid sampling engine no longer encodes interpretable kinetic information. This is particularly true if the engine is coupled to the replica exchange (REX) method (Sugita and Okamoto, 1999), as is done here. However, beyond describing sampling efficiency, kinetics are of no interest given that the potential energy function is artificial. Conversely, due to future applications in the presence of physical potentials, it is important to us that the thermodynamics be approximately correct. This requires that both IMD and MC portions sample from the same thermodynamic ensemble and use an identical or highly similar set of degrees of freedom. Further sources of error are found mostly in the IMD part, *i.e.*, the forces from the density restraint potential have to be correct, the integrator needs to be stable in the presence of the full potential at all strengths considered, and a source of (possibly colored) noise is found at the beginning of each IMD portion because of the requirement to assign velocities anew.

The implementation was realized entirely within the software package CAMPARI, and many additional details can be found in its public documentation at http://campari.sourceforge.net (accessed Sep. 1, 2013). A current development version of the code, which also includes the implementation of the density restraints required to reproduce the results in this manuscript, is available from the authors upon request (please send an e-mail to campari.software@gmail.com). For all simulations, the Metropolis MC segments are 600 elementary steps long, and the move sets in use build on our experience with MC simulations of biomolecules (Vitalis and Caflisch, 2010; Vitalis et al., 2008). We emphasize that the majority of move types offer two variants with differing amplitudes. The first samples uniformly from a local interval centered at the current position (referred to as “local” or “stepwise” moves below), while the second randomizes the degree of freedom with respect to the accessible space (referred to as “fully randomizing” moves below). This mixing of length scales is known to improve convergence rates for frustrated systems (Vitalis and Pappu, 2009). Parameters for individual systems are given below (see Test Systems). The formal temperature during MC sampling was 300K throughout. For all systems

studied, input files for CAMPARI specifying all auxiliary parameters for the move sets used to produce the data in this manuscript are available from the authors on request.

The implementation of the IMD portions uses a simple leap-frog integrator operating in mixed rigid-body / internal coordinate space coupled to the velocity rescaling thermostat (Bussi et al., 2007). The integration method is a new development to perform approximate dynamics simulations for these degrees of freedom. The approximation implies that, except for special cases, the evolution of the system violates Gauss's principle of least constraint or the conservation of angular momentum. The algorithm assumes a time-dependent, but diagonal mass (inertia) matrix for the internal and external degrees of freedom of each molecule, with instantaneous corrections applied to the velocities that keep the total energy approximately constant within this construct of assumptions. The diagonal mass matrix has the favorable property that degrees of freedom can be eliminated at will, which we utilize for the Arp2/3 system. In conjunction with a thermostat, the method generates canonical ensembles that yield thermodynamic properties, which for systems allowing simple comparisons are indistinguishable from more rigorous methodologies (an example being structural properties of liquid water when compared to Cartesian dynamics simulations with holonomic constraints (Miyamoto and Kollman, 1992)). Dynamical properties are often different, however, and this is expected. The framework for developing the method is probably most similar to that of Mazur (Mazur, 1997), but the algorithm itself is different. The obvious limitations regarding dynamics notwithstanding, it has the important advantage of not requiring correction terms for mass-metric tensor artifacts (Fixman, 1974). Details, derivations, and extensive tests of the integration scheme itself are reserved for a future publication.

For the purpose of assessment, we first point out that the MC acceptance rates are generally reasonable. They are above 5% for all move types employed for all conditions for all systems with the exception of rigid-body moves for the RNA stem-loop (see below). In particular, the essential MC moves, *viz*., pucker sampling moves for RNA and proline residues have acceptance rates ranging from ~10% to ~30%. It is important that these acceptance rates be reasonable, since convergence for the underlying

degrees of freedom could otherwise not be achieved. Ensemble correctness is guaranteed for the MC portion. For the IMD segments, we verified the correctness of analytical gradients by comparison to values obtained by finite differencing. From the actual simulations, we obtain average temperatures, both overall and individually for each degree of freedom. The former is usually within 0.2 K of the target of 300 K, whereas the latter have general errors of 2–5 K. All numbers are estimated crudely over 2 to 3×10^7 total steps. Torsional degrees of freedom with only hydrogen atoms rotating (*e.g.*, in alcohol groups) sometimes have larger errors of up to 20 K as expected on account of their low inertia and little relevance to the density restraint potential (weak coupling). The analysis of average temperatures for individual degrees of freedom also suggests that there are no equipartition artifacts affecting the simulations. To further test integrator stability, for all systems, we ran a few short simulations in the microcanonical ensemble at individual conditions and varying time steps, and we found the integrator to be quite stable for the overall potential function and input density used here. Specifically, this means that drift appeared negligible even for the time step used during production runs at mean temperatures close to 300 K. Of course, these are by no means rigorous tests, but they enforce our conjecture that the sampling engine is reasonable and yields unbiased results in a thermodynamic sense.

Energy Function

Aside from the potential term defined in eq. 4 of the main text, the Hamiltonian employed during the REX conformational sampling contains at most two other terms. First, select bonded potentials need to be included. For flexible polypeptides, these are taken from the OPLS-AA force field (Kaminski et al., 2001) to describe electronic structure-based terms, *e.g.*, the hindered rotation around the polypeptide backbone amide bond. For polynucleotides, bonded potentials are taken from the CHARMM27 force field (Mackerell Jr. et al., 2000) instead. The OPLS-AA parameters for proline bias the pucker state too much, and published modifications were applied (Radhakrishnan et al., 2012). The second additional term is only relevant for ubiquitin. Here, we included a weak statistical biasing potential to improve simulation convergence. For its derivation, we first performed pure MC simulations of all 18 relevant

dipeptides, *i.e.*, single residues capped with both acetyl (N) and *N*-methylamide (C) termini. These simulations employed a slightly modified version of the ABSINTH implicit solvation model and force field (Vitalis and Pappu, 2009). Importantly, the atomic radii represent by far the most important component for defining the accessible space and are exactly as published. Soft terms of the force field hardly matter due to a formal simulation temperature of 600 K. For charged side chains, a single counterion (sodium or chloride) was added. The move set included side chain, ω, ϕ/ψ pivot moves as well as rigid-body translation/rotation moves. MC moves facilitate conformational jumps, *e.g.*, regarding the left-hand and right-sides of ϕ/ψ space or *cis*/*trans* isomerizations of the peptide bond. Each simulation yielded 9.5×10^5 samples to derive a two-dimensional histogram in ϕ/ψ space, which was converted to a potential by taking the negative logarithm. A scaling factor in units of kcal/mol was incorporated to yield the potentials shown in Fig. S1. This factor was chosen to ensure that the potential is sufficiently discriminative.

REX Settings

Swap cycles were performed every 1000 steps for the flexible systems and every 200 steps for Arp2/3. In a swap cycle, we attempted $N_r - 1$ random neighbor exchanges including the possibility of the same neighbor pair being picked twice. Here, N_r is the number of replicas for a given run. Due to the sampling protocol, the majority of swap cycles occurred in IMD segments, and for successful swaps the velocities remained unchanged and associated with structures rather than conditions. The replicas differ in at most two parameters: the outside scaling factor for the density restraint potential, f_D, and the threshold input density, ω_t (the latter is explored only for ubiquitin). The resultant schedules never differ in both parameters for neighboring replicas. Acceptance rates for swap moves ranged from *ca*. 10% to well above 50 %.

TEST SYSTEMS (related to Experimental Procedures and Results – Test Systems)

Arp2/3

The MC portions of the simulations used only rigid-body moves. These sampled a single chain (50 %) or either 2 or 3 chains (25 % each). Maximum step sizes for local translation and rotation moves (70 %) were 0.4 Å and 2º, respectively. The IMD portions used a time step of 5 ps and a coupling time for the thermostat of 50 ps. The first 1.5×10^6 of the 1.15×10^7 total steps were discarded as equilibration and 1000 snapshots were recorded for each replica in each run.

Data analysis was performed for each REX trajectory independently (differing by values for f_D and the resolution of the input map). Clustering employed a recent tree-based algorithm (Vitalis and Caflisch, 2012) with settings of 10 Å for the threshold radius, a tree height of 10, and a coarsest radius of 80 Å. The distance function uses the RMSD between coordinate subsets sufficient to describe the assembly exactly. For this, we chose 3 distal sites on each domain. Specifically, these are the C_α atoms of residues E104, P265, and L315 in chain A, of residues T238, V273, and T293 in chain B, of residues R84, L146, and A276 in chain C, of residues N21, G135, and L277 in chain D, of residues S6, P31, and K88 in chain E, of residues V12, R32, and N167 in chain F, and of residues D15, G49, and S68 in chain G. The numbering refers to that in PDB entry 1TYQ. Because the density restraints provide an absolute reference in space, no coordinate alignment must be performed.

RNA Stem-Loop

The stem-loop has the sequence 5'-GpGpGpApCpCpUpUpCpCpApApGpUpCpUpC-3'. Due to treating the system as a flexible polymer, the MC portions of the simulations used different move types. The most important ones are those sampling the pucker angles of the nucleotide sugars (31.4 % of all moves). Stepwise pucker moves (80 % of all pucker moves) used maximum increments of 3º and 10º for bond and dihedral angles, respectively. Fully randomizing side chain moves (19.6 %) sampled at most two dihedral angles in the same residue concurrently. Rigid body moves (2 %) employed step

sizes for local moves (70 % of all rigid body moves) of 0.8 Å and 10º, respectively. These values are too large explaining the low acceptance rates alluded to above. The remaining moves were pivot moves on single nucleic acid backbone torsions, either stepwise (15º, 90 %) or fully randomizing. The IMD portions used a time step of 10 fs and a coupling time for the thermostat of 1 ps. The first 1.2×10^7 steps of the 1.6×10^8 total steps were discarded as equilibration, and 29600 snapshots were recorded for each replica in each run.

Data analysis was carried out independently for each REX trajectory (the trajectories differ by their values for f_D and the resolution of the input map). The clustering was performed with settings of 2 Å for the threshold radius, a tree height of 10, and a coarsest radius of 12 Å. Distance evaluations utilized the RMSD between coordinate sets comprised of all heavy atoms. This is possible because there are no moieties with identical substituents to exclude.

Ubiquitin

The MC portions of the simulations used different move types. The most important ones are probably those sampling the pucker angles of the 3 proline residues as these cannot be sampled by IMD (7.5 % of all moves). Stepwise pucker moves (90 % of all pucker moves) used maximum increments of 1º and 3º for bond and dihedral angles, respectively. Fully randomizing side chain moves (4.9 %) sampled at most three dihedral angles in the same residue concurrently. Dedicated pivot moves (8.4 %) sampled the ω bonds with a maximum step size of 2º for the fraction of them (90 %) that were local perturbations. We included an implementation of concerted rotation moves (9.3 %) combining exact closure using the ϕ/ψ dihedral angles of 3 consecutive residues with a biased pre-rotation move (Dinner, 2000; Favrin et al., 2001). The pre-rotation segments sampled between 3 and 8 degrees of freedom. Rigid body moves were separated into rotation (1.4 %) and translation (0.6 %) moves with employed maximum step sizes for local moves (70 % of each respective subset) of 0.4 Å and 2º, respectively. The remaining moves (the majority) were pivot moves on ϕ/ψ pairs for individual

residues, either stepwise (10º, 80 %) or fully randomizing. The IMD portions used a time step of 10 fs and a coupling time for the thermostat of 1 ps.

The REX schedule is more complex for ubiquitin. Each run is comprised of 48 replicas with 12 different values for f_D and 4 different values for ω_t. Replicas are arranged such that f_D increases from 0.043 via 0.045, 0.048, 0.051, 0.055, 0.059, 0.063, 0.066, 0.069, 0.072, and 0.075, to 0.080 for replicas 1 to 12 and 25 to 36. It decreases by the inverted schedule for replicas 13 to 24 and 37 to 48. Conversely, ω_t is constant for replicas in blocks of 12 at values of -0.225, -0.215, -0.205, and -0.195. These values yield a narrow range of mean molecular densities (M_M/V_M, see eq. S2) of 1.75 to 1.88 g cm^{-3}. There are 4 identical sets of these simulations. The first 7.2×10^7 steps of the 1.72×10^8 total steps per replica were discarded as equilibration, and 10000 snapshots were recorded for each replica in each run.

For RMSD calculations outside of clustering analysis, we used an atom set composed of all atoms with only those removed that could give rise to spurious signals on account of symmetry. This means discarding all atoms corresponding to identical substituents at any given atom (*e.g.*, terminal carbon atoms in valine side chains). The resultant set retains 620 of 746 atoms. Data of this type are used in Figs. 3 and 4. Because initial inspection of the data revealed poor convergence on account of persistent differences between runs in the average restraint energies, most analysis was carried out on combined trajectories. For this, we concatenated all individual trajectories with f_D values of at least 0.059. RMSD autocorrelation traces as well as initial clustering results (not shown) revealed that simulations for lower f_D values are unlikely to contribute to well-defined clusters. Trajectory concatenation implied that we needed to recompute restraint energies to make values coming from different replicas comparable. For this, we used settings of $f_D = 0.08$ and $\omega_t = -0.190$. These data are used in Figs. 3a-b.

Clustering was performed with settings of 2.5 Å for the threshold radius, a tree height of 10, and a coarsest radius of 15 Å. Distance evaluations utilized the RMSD between coordinate sets comprised of

selected atoms chosen to keep dimensionality tractable and again to avoid problems with moieties carrying identical substituents. The backbone atoms used were nitrogen and oxygen. In addition we picked one or two side chain atoms. C_β was chosen for valine, C_γ for aspartate and leucine, and C_δ for glutamate. In all those cases, this is because of the chemical equivalence of the terminal atoms. Isoleucine does not offer this symmetry and both terminal carbon atoms were consequently part of the set. For the amides, asparagine and glutamine, both the side chain amide oxygen and nitrogen atoms were picked, whereas for the alcohols, serine and threonine, only their oxygen atoms were included. During clustering, we did not want to overemphasize the large range of positions accessible to the positively charged side chains and chose the C_γ and C_ζ atoms for lysine and arginine, respectively. Proline and alanine have very little freedom and we selected the C_γ and C_β atoms for those two cases. The aromatic side chains are rigid and represented well by picking the C_ζ atom only for phenylalanine, the C_ζ and phenol oxygen atoms for tyrosine, and both imidazole nitrogen atoms for histidine. Finally, the sulfur atom was included for methionine.

SUPPLEMENTAL REFERENCES

Bussi, G., Donadio, D., and Parrinello, M. (2007). Canonical sampling through velocity rescaling. J. Chem. Phys. *126,* 14101.

Dinner, A.R. (2000). Local deformations of polymers with nonplanar rigid main-chain internal coordinates. J. Comput. Chem. *21,* 1132–1144.

Favrin, G., Irbäck, A., and Sjunnesson, F. (2001). Monte Carlo update for chain molecules: Biased Gaussian steps in torsional space. J. Chem. Phys. *114,* 8154–8158.

Fixman, M. (1974). Classical statistical mechanics of constraints: A theorem and application to polymers. Proc. Natl. Acad. Sci. USA *71,* 3050–3053.

Kaminski, G.A., Friesner, R.A., Tirado-Rives, J., and Jorgensen, W.L. (2001). Evaluation and reparametrization of the OPLS-AA force field for proteins via comparison with accurate quantum chemical calculations on peptides. J. Phys. Chem. B *105,* 6474–6487.

Mackerell Jr., A.D., Banavali, N., and Foloppe, N. (2000). Development and current status of the CHARMM force field for nucleic acids. Biopolymers *56,* 257–265.

Mazur, A.K. (1997). Quasi-Hamiltonian equations of motion for internal coordinate molecular dynamics of polymers. J. Comput. Chem. *18,* 1354–1364.

Miyamoto, S., and Kollman, P.A. (1992). SETTLE: An analytical version of the SHAKE and RATTLE algorithm for rigid water models. J. Comput. Chem. *13,* 952–962.

Sugita, Y., and Okamoto, Y. (1999). Replica-exchange molecular dynamics method for protein folding. Chem. Phys. Lett. *314,* 141–151.

Vitalis, A., and Caflisch, A. (2010). Micelle-like architecture of the monomer ensemble of Alzheimer's amyloid-β peptide in aqueous solution and its implications for Aβ aggregation. J. Mol. Biol. *403,* 148–165.

Vitalis, A., and Pappu, R.V. (2009). Methods for Monte Carlo simulations of biomacromolecules. Annu. Rep. Comput. Chem. *5,* 49–76.

Vitalis, A., Wang, X., and Pappu, R.V. (2008). Atomistic simulations of the effects of polyglutamine chain length and solvent quality on conformational equilibria and spontaneous homodimerization. J. Mol. Biol. *384,* 279–297.

MOVIE S1 (RELATED TO FIGURE 2): The heavy atoms of the RNA stem-loop are shown colored from red to blue via green (5' to 3') in stick representation. Faces of sugars and nucleotides bases are colored separately. The movie shows a section of a trajectory (200 ns) continuous in geometry, *i.e.*, the REX condition (value of f_D) varies and is displayed at the top left. These data are from the run with higher resolution input data. The system is initially trapped in a misfold. By excursion into replicas with low restraint strength, it escapes and enters additional traps (*e.g.*, 20 s, 40 s), until an extended stay at low f_D (50 to 75 s) allows it to find a native-like conformation. The favorable restraint energy leads to an immediate drift toward replicas with higher f_D.